Contribution from the Groupe Magnétisme et Diffusion par Interactions Hyperfines and Laboratoires de Chimie, UA CNRS 321, Département de Recherche Fondamentale, Centre d'Etudes Nucléaires, 85 X, F-38041 Grenoble Cedex, France

Correlation among the Structural, Electronic, and Magnetic Properties of $[Fe_4(\mu_3\text{-}S)_3(\mu_3\text{-}S_2)Cp_4]^{n+}$ (n = 0–2) Clusters at Various Oxidation States

N. Dupré,[1b] P. Auric,[1a] H. M. J. Hendriks,[1b,c] and J. Jordanov*[1b]

Received August 19, 1985

The series $[Fe_4(\mu_3\text{-}S)_3(\mu_3\text{-}S_2)Cp_4]^{n+}$, with n = 0 (I), 1 (II), and 2 (III), was examined in order to put into evidence the relationship between the core geometry and the electronic distribution, when the overall oxidation state is varied. The crystal structure of $[Fe_4(\mu_3\text{-}S)_3(\mu_3\text{-}S_2)Cp_4][PF_6]_2\cdot EtOH$ (III) is described in detail. Complex III ($C_{22}H_{26}F_{12}Fe_4OP_2S_5$) crystallizes in the orthorhombic space group *Pbca* with cell constants a = 13.494 (3) Å, b = 27.193 (8) Å, c = 17.529 (6) Å, V = 6432.2 Å^3, and Z = 8. Refinement by full-matrix least squares of 431 parameters on 4666 data gave a final R value of 0.064. The Fe_4S_5 core is retained, as in the monocation. A significant contraction of two Fe–Fe distances has occurred however, from 2.723 and 2.866 Å in II to 2.661 and 2.650 Å in III. Moreover, a higher local symmetry is present in the dication at the Fe(2) site, where a diagonal mirror plane bisects the dihedral angle defined by the two core faces Fe(2), S(5), Fe(4) and Fe(2), S(5), Fe(1). Comparative analysis over the series shows that, upon successive reduction (or oxidation), the most significant structural changes occur at Fe(1), Fe(2), and Fe(4) but not at the five-coordinated Fe(3) site. Zero-field Mössbauer spectra of compounds I, II, and III at 1.8 K consist of three quadrupole doublets of 2:1:1 relative intensities. The average isomer shift values of the three tetracoordinated iron sites decrease upon oxidation, whereas the five-coordinated iron remains essentially unaffected by the same process. Mössbauer spectra of the paramagnetic monocation at 1.8 K with applied magnetic fields (H_0 < 100 kOe) indicate the presence of a very small (less than 10 kOe) hyperfine field at the iron nuclei. No isotropic shifts of the cyclopentadienyl resonances in the ^1H and ^{13}C NMR spectra of compound II are detected. These observations led us to conclude that the unpaired electron spin density must be predominantly localized on the sulfur atoms of the Fe_4S_5 core.

Introduction

A number of non-heme Fe–S proteins are known, such as the Fe–Mo protein of nitrogenase and the ferredoxin from *Bacillus stearothermopilus*, that exhibit somewhat unusual electronic properties. These properties, which appear mainly from ^{57}Fe Mössbauer and EPR spectra,[2-4] suggest that the iron atoms in the Fe_4S_4 core are not precisely equivalent. Such inequivalencies may be accounted for by the protein structure itself, but also by replacement of the thiolate terminal ligands by other nucleophiles or by expansion to five-coordination for some of the iron sites. This led to a number of efforts to isolate Fe_4S_4 units with iron atoms having different ligands and different coordination geometries for the purpose of ascertaining the effects of ligand and structural variations on the $[Fe_4S_4]$ core properties. Thus, $[Fe_4S_4Cl_4]^{2-}$[5] was first reported, followed by $[Fe_4S_4(OPh)_4]^{2-}$[6a,b] and $[Fe_4S_4(SPh_2)(o\text{-tol})_2]^{2-}$.[6c,d] Recently also $[Fe_4S_4X_{4-n}(Et_2dtc)_n]^{2-}$[7] (X = Cl^-, PhS^-) and $[Fe_4S_4(SC_6H_4\text{-}o\text{-}OH)_4]^{2-}$[8] have been synthesized, which contain either two or one pentacoordinated iron atom within the same core.

In the course of our investigations of the reactivity of $Fe_4S_6Cp_4$, an Fe–S cluster with two S_2^{2-} groups, vs. Mo complexes at various oxidation states, we reported on the isolation and structure determination[9] of $[Fe_4(\mu_3\text{-}S)_3(\mu_3\text{-}S_2)Cp_4][MoOCl_4(thf)]$. The X-rays analysis revealed a distorted Fe_4S_4 core, where one Fe, out of the four, has expanded its coordination number to five. It became then important for us to try and establish a correlation between geometry and electronic configuration, namely to investigate whether this structurally different iron site induces any modification of the electronic distribution within the cluster core. Moreover, both the reduced and oxidized parent clusters being available,[10] it was of interest to extend the structure–bonding comparison to the overall cluster oxidation state.

This paper presents an account of the magnetic and Mössbauer spectroscopic properties of $[Fe_4(\mu_3\text{-}S)_3(\mu_3\text{-}S_2)Cp_4]^{n+}$ (n = 0–2), hereafter designated I–III, respectively, together with the results of an X-ray diffraction analysis of the dication tetrakis(π-cyclopentadienyl)pentasulfidotetrairon bis(hexafluorophosphate)–ethanol and some conclusions of an Fe-EXAFS study[11] of the neutral homologue, which implies that the overall Fe–S core structure seems to be retained.

Table I. Summary of Data Collection and Structure Refinement for $[Fe_4(\mu_3\text{-}S)_3(\mu_3\text{-}S_2)Cp_4][PF_6]_2\cdot EtOH$

empirical formula	$C_{22}H_{26}F_{12}Fe_4OP_2S_5$
cryst dimens, mm	0.4 × 0.4 × 0.5
space group	*Pbca*
a, Å	13.494 (3)
b, Å	27.193 (8)
c, Å	17.529 (6)
$\alpha = \beta = \gamma$, deg	90
V, Å^3	6432.2
molecules/cell	8
d_{calcd}, g/cm^3	2.02
λ, Å	0.7107
linear abs coeff, cm^{-1}	23.2
transmission factors	
min	0.82
max	1.00
total no. of reflcns collcd ($1° < \theta < 35°$)	8263
no. of reflcns used (rejection criterion)	4666 ($I > 3\sigma(I)$)
no. of variables	431
final residuals	
$R(F)$	0.064
$R_w(F)$	0.065

(1) (a) Groupe Magnétisme et Diffusion par Interactions Hyperfines. (b) Laboratoires de Chimie, UA CNRS 321. (c) Postdoctoral Fellow 1981–1982.
(2) (a) Münck, E.; Rhodes, H.; Orme-Johnson, W. H.; Davis, L. C.; Brill, W. J.; Shah, V. K. *Biochim. Biophys. Acta* **1975**, *400*, 32. (b) Zimmermann, R.; Münck, E.; Brill, W. J.; Shah, V. K.; Henzl, M. T.; Rawlings, J.; Orme-Johnson, W. H. *Ibid.* **1978**, *537*, 185. (c) Huynh, B. H.; Henzl, M. T.; Christner, J. A.; Zimmermann, R.; Orme-Johnson, W. H.; Münck, E. *Ibid.* **1980**, *623*, 124.
(3) Smith, B. E.; O'Donnell, M. J.; Lang, G.; Spartalian, K. *Biochem. J.* **1980**, *191*, 449.
(4) Mullinger, R. N.; Cammack, R.; Rao, K. K.; Hall, D. O.; Dickson, D. P. E.; Johnson, C. E.; Rush, J. D.; Simopoulos, A. *Biochemistry* **1975**, *151*, 75.
(5) Bobrik, M. A.; Hodgson, K. O.; Holm, R. H.; *Inorg. Chem.* **1977**, *16*, 1851.
(6) (a) Cleland, W. E.; Averill, B. A. *Inorg. Chim. Acta* **1981**, *56*, L9. (b) Cleland, W. E.; Holtman, D. A.; Sabat, M.; Ibers, J. A.; DeFotis, G. C.; Averill, B. A. *J. Am. Chem. Soc.* **1983**, *105*, 6021. (c) Coucouvanis, D.; Kanatzidis, M.; Simhon, E.; Baenziger, N. C. *J. Am. Chem. Soc.* **1982**, *104*, 1874. (d) Kanatzidis, M. G.; Baenziger, N. C.; Coucouvanis, D.; Simopoulos, A.; Kostikas, A. *Ibid.* **1984**, *106*, 4500.
(7) (a) Kanatzidis, M. G.; Ryan, M.; Coucouvanis, D.; Simopoulos, A.; Kostikas, A. *Inorg. Chem.* **1983**, *22*, 181. (b) Kanatzidis, M. G.; Coucouvanis, D.; Simopoulos, A.; Kostikas, A.; Papaefthymiou, V. *J. Am. Chem. Soc.* **1985**, *107*, 4925.
(8) Johnson, R. E.; Papaefthymiou, G. C.; Frankel, R. B.; Holm, R. H. *J. Am. Chem. Soc.*, **1983**, *105*, 7280.
(9) Dupré, N.; Hendriks, H. M. J.; Jordanov, J.; Gaillard, J.; Auric, P. *Organometallics* **1984**, *3*, 800.
(10) Kubas, G. J.; Vergamini, P. J. *Inorg. Chem.* **1981**, *20*, 2667.
(11) Diakun, G.; Dupré, N.; Jordanov, J., manuscript in preparation.

0020-1669/86/1325-1391$01.50/0

Experimental Section

Compounds I–III were prepared as previously described[9,10] under an argon atmosphere, with use of Schlenk-type apparatus and of distilled and degassed solvents. All samples were prepared and all measurements were performed under anaerobic conditions.

Measurements. Mössbauer spectra were recorded at several temperatures using conventional constant acceleration spectrometers employing 25 mCi of ^{57}Co in a rhodium matrix maintained at room temperature. Spectra with external fields were obtained by using a superconducting solenoid with longitudinal geometry. The source (100 mCi) was kept at 4.2 K whereas the absorber temperature varied from 1.8 to 300 K. Magnetic susceptibility measurements were carried out on a SHE SQUID magnetometer. Several runs with different containers and different samples of the same compound were made in order to ensure reproducibility of results. Diamagnetic corrections were applied by using values from a standard source.[12] Magnetization measurements were made at 6 K and from 0.1 to 45 kG.

^{13}C NMR spectra were recorded on a Bruker CXP 200 spectrometer at 50.3 MHz by using magic-angle spinning (MAS) and cross-polarization (CP) techniques.[13] The solid samples were about 250 mg. The samples rotation speed varied within the range 3200–3500 Hz, the CP time being 3 ms and the time repetition between each scan being 5 s. The spectra extend over 30 KHz. A polyethylene spherule was used for isomer shift calibration (δ_{PE} = 33.6 ppm).

X-ray Data Collection and Reduction. Dark-brown, air-stable crystals were obtained when an acetonitrile solution (50 mL) of $[Fe_4(\mu_3\text{-}S)_3(\mu_3\text{-}S_2)Cp_4](PF_6)_2$ (0.4 g) was treated with dichloromethane (100 mL) and ethanol (100 mL) and left overnight at room temperature. Preliminary Weissenberg photographs indicated Laue symmetry *mmm*, and the systematic absences identified the space group as *Pbca*. Pertinent details on crystal data and collection of intensity data are given in Table I. The cell parameters were determined by least squares refinement of the angular settings of 14 reflections with $7° \leq \theta \leq 13°$. Intensity data were collected at room temperature on a Nonius CAD-4 diffractometer (ω scans) for all reflections with $1° < \theta < 35°$ and $h > 0$, $k > 0$ and $l > 0$. Graphite-monochromated Mo Kα radiation was used. The scan speeds were determined by a required precision of $\sigma(I)/I < 0.02$ with a maximum scan time of 100 s. Each reflection was measured in 96 steps, 16 of which at each end of the scan profile were considered as background. Intensities I and their standard deviations $\sigma(I)$ were assigned as $I = S[P - 2(B_1 + B_2)]$ and $\sigma(I) = S[P + 4(B_1 + B_2)]^{1/2}$, where S is the scan rate, p is the scan count, and B_1 and B_2 are the low- and high-angle background counts. Three standard reflections were measured after every 10800 s of radiation time to check for instrumental instability and crystal decomposition; no significant change in their intensities was observed. A semiempirical absorption correction was applied,[14] and the intensities were corrected for Lorentz and polarization effects but not for extinction. Scattering factors for neutral atoms were taken from ref 15, and those for Fe, S, and P were corrected for the real and imaginary parts of anomalous dispersion.[16]

Structure Solution and Refinement. The structure was solved with the direct-methods program MULTAN.[17] All atoms of the $[Fe_4(\mu_3\text{-}S)_3(\mu_3\text{-}S_2)Cp_4]^{2+}$ cation are symmetry-independent. The solution (based on 284 reflections with $|E| > 1.75$) with the highest figure of merit revealed the position of all independent Fe, S, and P atoms in the structure. After a least-squares refinement and subsequent Fourier map, all the cyclopentadienyl carbon atoms were found.

A series of least-squares refinements and Fourier and difference Fourier maps suggested that the hexafluorophosphate anions are seriously disordered: many peaks were found at a distance of 1.5–1.75 Å from the P atoms. These peaks were included in the refinement as partially occupied F atoms with fixed isotropic thermal parameters of B = 6.0 Å^2; their multiplicities were refined. Those F atoms whose multiplicities dropped under 0.10 were skipped from the refinement. This procedure led eventually to 31 partially occupied F atoms (14 around P_1 and 17 around P_2) with multiplicities ranging from 0.14 to 0.55. At this stage, a difference Fourier map revealed the presence of an ethanol solvent molecule.

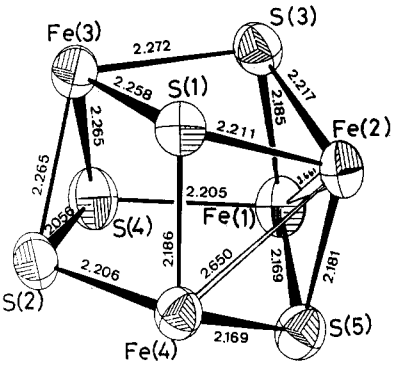

Figure 1. ORTEP drawing of the Fe_4S_5 core of the $[Fe_4(\mu_3\text{-}S)_3(\mu_3\text{-}S_2)Cp_4]^{2+}$ dication. Thermal ellipsoids are plotted at the 50% level.

The structure was further refined in several full-matrix least-squares cycles. All non-fluorine atoms were refined anisotropically; hydrogen atoms have not been included. During the last cycle of the refinement, the parameter shifts were less than 4% of their esd for the cation atoms and less than 40% of their esd for the ethanol and anion atoms. A final difference Fourier map showed some electron density in the region of the PF_6 anions. These peaks most likely represent also parts of the disordered F atoms, but they have not been included in the refinement. Also, some electron density was found near the ethanol atoms, suggesting a small disorder; The final residuals are $R = \sum(|F_o| - |F_c|)/\sum|F_o| = 0.064$ and $R_w = [\sum w(|F_o| - |F_c|)^2/\sum w|F_o|^2]^{1/2} = 0.065$, w being defined as $w = 1/\sigma^2(F_o)$. Final positional atomic parameters appear in Table II. A list of observed and calculated structure factors is available as supplementary material, as well as the anisotropic thermal parameters.

Results

Description of the Structure of $[Fe_4(\mu_3\text{-}S)_3(\mu_3\text{-}S_2)Cp_4][PF_6]_2 \cdot EtOH$ (III). Compound III contains discrete $[Fe_4(\mu_3\text{-}S)_3(\mu_3\text{-}S_2)Cp_4]^{2+}$ dications and $[PF_6]^-$ anions. Figure 1 displays the configuration of the Fe_4S_5 framework of the dication, and Table III shows selected bond lengths and angles. The structural analysis reveals that the dication retains the overall distorted cubane-like Fe_4S_5 framework already evidenced by us[9] for the monocation homologue. The presence of the S_2 ligand "side-on" bonded to Fe(3) induces pentacoordination at the latter and distortion from a conventional Fe_4S_4 core.

As a consequence, three different types of iron atoms are present: (a) Fe(3) is bonded to four sulfur atoms but is not involved in any bonding interaction with the other iron atoms; (b) Fe(1) and Fe(4) are both bonded to three sulfur atoms and involved in one Fe–Fe bond each; (c) Fe(2) is also bonded to three sulfur atoms and interacts with two other iron atoms.

The six Fe–Fe distances divide into three different sets: two bonding lengths of 2.650 (1) and 2.661 (1) Å; three nonbonding lengths with mean value 3.394 Å, and another nonbonding length at 3.641 Å. The 13 Fe–S bond lengths split into two sets: one set of nine Fe–S bonds spread between 2.169 (2) and 2.217 (2) Å involving the three irons that retain the usual tetrahedral-like environment and one set of four Fe–S bonds spread between 2.258 (2) and 2.272 (2) Å corresponding to the five-coordinated Fe(3) site. The latter sits at the apex of a square pyramid made up by the four S ligands and distorted by the presence of the S(2)–S(4) bond, which induces a smaller S(2)–Fe(3)–S(4) angle (53.9°) than the three other S–Fe(3)–S angles (averge value 76.6°). The remaining nine S–Fe–S bond angles are spread over a range from 77.2 to 102.1°. The 11 Fe–S–Fe bond angles split into three distinct sets: one set of four angles of average 74.8°, one set of six angles of average 98.9°, which are values similar to those found in analogous Fe–S clusters,[18,19] and one larger angle at 114.14°.

(12) Landolt-Börnstein *Numerical Data and Functional Relationships in Science and Technology*; König, E., Ed.; Springer-Verlag: West Berlin, 1966; Vol. II-2.
(13) (a) Maciel, G. E. *Science (Washington, D.C.)* **1984**, *226*, 282. (b) Harris, R. K. In *Nuclear Magnetic Resonance Spectroscopy*; Harris, R. K., Ed.; Pitman: London, 1983; Chapter 6.
(14) A locally written program was used, based on the method described in: Kopfmann, G.; Huber, R. *Acta Crystallogr., Sect. A: Cryst. Phys., Diffr., Theor. Gen. Chem.* **1968**, *A24*, 348.
(15) *International Tables for X-ray Crystallography*; Kynoch: Birmingham, England, 1969; Vol. I, p 105.
(16) Real and imaginary parts of anomalous dispersion corrections were taken from: *International Tables for X-ray Crystallography*; Kynoch: Birmingham, England, 1969; Vol. I, pp 149–150.
(17) Germain, G.; Main, P.; Woolfson, M. M. *Acta Crystallogr.* **1971**, *127*, 368.
(18) (a) Trinh-Toan; Fehlhammer, W. P.; Dahl, L. F. *J. Am. Chem. Soc.* **1977**, *99*, 402. (b) Trinh-Toan; Teo, B. K.; Ferguson, J. A.; Meyer, T. J.; Dahl, L. F. *Ibid.* **1977**, *99*, 408.

Table II. Positional Parameters of $[Fe_4(\mu_3\text{-}S)_3(\mu_2\text{-}S_2)Cp_4][PF_6]_2\cdot EtOH$ and Multiplicities of the Fluorine Atoms[a] with Their Estimated Standard Deviations in Parentheses

atom[b]	$10^4x/a$	$10^4y/b$	$10^4z/c$	atom[c]	$10^4x/a$	$10^4y/b$	$10^4z/c$	mult
Fe(1)	7167 (1)	5634 (1)	5303 (1)	F(101)	2875 (9)	5324 (5)	2816 (8)	0.554 (13)
Fe(2)	7643 (1)	6528 (1)	5802 (1)	F(102)	3678 (16)	5960 (7)	3497 (13)	0.345 (14)
Fe(3)	9278 (1)	5638 (1)	6354 (1)	F(103)	1844 (11)	5874 (6)	2293 (10)	0.441 (13)
Fe(4)	9227 (1)	6462 (1)	4913 (1)	F(104)	2923 (12)	6460 (6)	2548 (10)	0.444 (13)
S(1)	9208 (2)	6458 (1)	6160 (2)	F(105)	7350 (13)	3529 (7)	6807 (11)	0.368 (11)
S(2)	9752 (2)	5705 (1)	5118 (2)	F(106)	7407 (17)	4574 (8)	6734 (15)	0.308 (14)
S(3)	7644 (2)	5829 (1)	6455 (2)	F(107)	7346 (22)	4374 (10)	7899 (15)	0.233 (11)
S(4)	8592 (2)	5238 (1)	5351 (2)	F(108)	7815 (10)	4193 (5)	6440 (8)	0.477 (11)
S(5)	7721 (2)	6248 (1)	4637 (2)	F(109)	7181 (19)	3874 (9)	6365 (14)	0.273 (12)
C(11)	9386 (9)	4354 (6)	324 (14)	F(110)	6731 (21)	3760 (13)	7771 (17)	0.248 (14)
C(12)	9076 (11)	4387 (7)	−422 (11)	F(111)	8333 (12)	3969 (6)	7212 (12)	0.391 (13)
C(13)	8514 (9)	4834 (6)	−487 (9)	F(112)	6036 (13)	4181 (6)	6937 (14)	0.401 (14)
C(14)	8524 (8)	5051 (4)	220 (9)	F(113)	6633 (16)	4154 (8)	7994 (12)	0.339 (13)
C(15)	9033 (10)	4778 (7)	722 (8)	F(114)	6128 (22)	4092 (11)	7519 (22)	0.230 (12)
C(21)	7955 (9)	2783 (4)	420 (7)	F(201)	905 (4)	3433 (9)	1048 (13)	0.349 (15)
C(22)	7349 (8)	2703 (4)	1069 (8)	F(202)	2813 (13)	3858 (6)	537 (8)	0.505 (14)
C(23)	7760 (11)	2988 (5)	1674 (7)	F(203)	2150 (13)	3124 (8)	408 (11)	0.415 (18)
C(24)	8647 (9)	3227 (4)	1370 (9)	F(204)	2281 (11)	3611 (8)	1889 (8)	0.507 (18)
C(25)	8730 (8)	3093 (4)	605 (9)	F(205)	8428 (28)	9030 (11)	4034 (18)	0.309 (18)
C(31)	4443 (7)	4297 (4)	2025 (6)	F(206)	8014 (27)	9112 (12)	3650 (27)	0.231 (17)
C(32)	4411 (9)	4759 (5)	1647 (7)	F(207)	8830 (16)	8240 (7)	3576 (14)	0.408 (17)
C(33)	5262 (10)	5038 (4)	1885 (7)	F(208)	8862 (35)	8547 (19)	4654 (29)	0.140 (13)
C(34)	5822 (8)	4743 (5)	2390 (8)	F(209)	7548 (13)	7955 (6)	3932 (10)	0.406 (12)
C(35)	5325 (8)	4282 (4)	2481 (6)	F(210)	8179 (33)	7977 (15)	3533 (23)	0.168 (12)
C(41)	5827 (8)	3043 (4)	−1012 (7)	F(211)	8871 (20)	8822 (12)	4256 (16)	0.293 (16)
C(42)	5127 (9)	3425 (4)	−1166 (6)	F(212)	6824 (16)	8623 (9)	4111 (15)	0.303 (13)
C(43)	4391 (8)	3389 (4)	−590 (7)	F(213)	3136 (11)	3345 (6)	1345 (10)	0.410 (12)
C(44)	4626 (8)	3003 (4)	−76 (6)	F(214)	7828 (19)	8899 (16)	3249 (18)	0.276 (17)
C(45)	5518 (8)	2782 (4)	−353 (7)	F(215)	7772 (45)	9030 (16)	4282 (27)	0.163 (14)
P(1)	2801 (3)	5920 (2)	2847 (3)	F(216)	8076 (14)	8346 (8)	4842 (11)	0.422 (18)
P(2)	2922 (2)	6488 (2)	6023 (2)	F(217)	1587 (32)	3334 (15)	1811 (24)	0.185 (15)
O(100)	−153 (7)	8143 (3)	6023 (5)					
C(101)	518 (20)	8063 (8)	6736 (11)					
C(102)	230 (18)	7595 (7)	7194 (10)					

[a] The fluorine atoms have been refined with a fixed isotropic thermal parameter of $B = 6.0$ Å^2. [b] The Fe and S atom numbering is given in Figure 1. The first digit of the C atom numbering corresponds to the parent Fe atom. [c] The first digit of the atom number corresponds to the parent phosphorus atom.

Table III. Selected Geometric Parameters for $[Fe_4(\mu_3\text{-}S)_3(\mu_3\text{-}S_2)Cp_4]^{2+}$

	Bond Lengths (Å)		
Fe(1)–S(3)	2.185 (2)	Fe(4)–S(1)	2.186 (2)
Fe(1)–S(4)	2.205 (2)	Fe(4)–S(2)	2.206 (2)
Fe(1)–S(5)	2.169 (2)	Fe(4)–S(5)	2.169 (2)
Fe(2)–S(1)	2.211 (2)	S(2)–S(4)	2.056 (3)
Fe(2)–S(3)	2.217 (2)	Fe(1)–Fe(2)	2.661 (1)
Fe(2)–S(5)	2.181 (2)	Fe(2)–Fe(4)	2.650 (1)
Fe(3)–S(1)	2.258 (2)	Fe(1)–Fe(3)	3.392 (1)
Fe(3)–S(2)	2.265 (2)	Fe(1)–Fe(4)	3.641 (1)
Fe(3)–S(3)	2.272 (2)	Fe(2)–Fe(3)	3.414 (1)
Fe(3)–S(4)	2.265 (2)	Fe(3)–Fe(4)	3.377 (1)
	Bond Angles (deg)		
S(5)–Fe(1)–S(3)	102.05 (9)	Fe(2)–S(1)–Fe(3)	99.63 (8)
S(5)–Fe(1)–S(4)	95.52 (9)	Fe(4)–S(1)–Fe(3)	98.89 (9)
S(3)–Fe(1)–S(4)	80.02 (8)	Fe(4)–S(1)–Fe(2)	74.14 (7)
S(5)–Fe(2)–S(1)	100.98 (8)	Fe(4)–S(2)–Fe(3)	98.06 (9)
S(5)–Fe(2)–S(3)	100.63 (9)	Fe(1)–S(3)–Fe(3)	99.09 (9)
S(1)–Fe(2)–S(3)	77.24 (8)	Fe(2)–S(3)–Fe(3)	99.01 (8)
S(1)–Fe(3)–S(2)	77.79 (8)	Fe(1)–S(3)–Fe(2)	74.37 (8)
S(1)–Fe(3)–S(3)	75.20 (8)	Fe(1)–S(4)–Fe(3)	98.69 (9)
S(4)–Fe(3)–S(3)	76.93 (8)	Fe(1)–S(5)–Fe(2)	75.43 (8)
S(4)–Fe(3)–S(2)	53.97 (8)	Fe(4)–S(5)–Fe(2)	75.07 (7)
S(1)–Fe(3)–S(4)	109.89 (8)	Fe(1)–S(5)–Fe(4)	114.14 (10)
S(2)–Fe(3)–S(3)	109.24 (8)	S(4)–S(2)–Fe(4)	111.37 (11)
S(5)–Fe(4)–S(1)	102.15 (9)	S(4)–S(2)–Fe(3)	63.01 (9)
S(5)–Fe(4)–S(2)	94.96 (8)	S(2)–S(4)–Fe(1)	110.73 (11)
S(1)–Fe(4)–S(2)	80.59 (8)	S(2)–S(4)–Fe(3)	63.01 (9)

Thus, the Fe_4S_5 core of the cation has a quite distorted geometry. Some degree of symmetry is however retained at the Fe(2) site, in the sense that a diagonal mirror plane exists, including S(5), Fe(2), and Fe(3), in the middle of the dihedral angle defined by the two faces Fe(2), S(5), Fe(4) and Fe(2), S(5), Fe(1). On either side of this mirror plane, the Fe–S bond lengths are almost identical (2.211 and 2.217 Å for Fe(2)–S(1) and Fe(2)–S(3)) and the two Fe–Fe bonding interactions are very similar (2.650 and 2.661 Å for Fe(2)–Fe(4) and Fe(2)–Fe(1)). The same goes for the angles: 100.98 and 100.63° for S(1)–Fe(2)–S(5) and S-

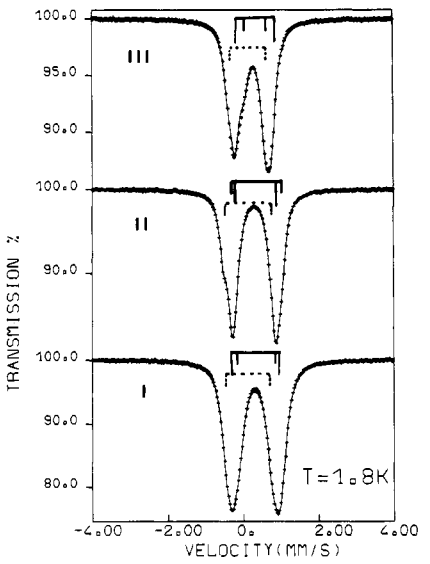

Figure 2. Zero-field Mössbauer spectra of $Fe_4(\mu_3\text{-}S)_3(\mu_3\text{-}S_2)Cp_4$ (I), $[Fe_4(\mu_3\text{-}S)_3(\mu_3\text{-}S_2)Cp_4][PF_6]$ (II), and $[Fe_4(\mu_3\text{-}S)_3(\mu_3\text{-}S_2)Cp_4][PF_6]_2$ (III). The solid lines are least-squares fits of the data. The dotted line represents the Fe(3) doublet.

(19) Mascharak, P. K.; Hagen, K. S.; Spence, J. T.; Holm, R. H. *Inorg. Chim. Acta* **1983**, *80*, 157.

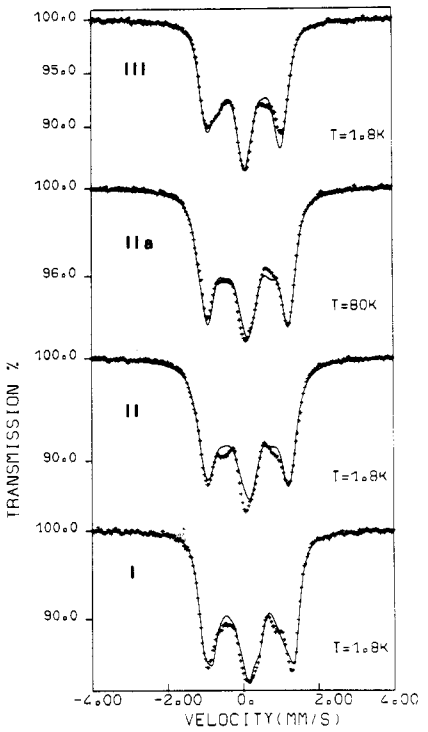

Figure 3. Mössbauer spectra of I–III at H_0 = 40 kOe. The solid lines are theoretical, assuming $H_n = H_0$.

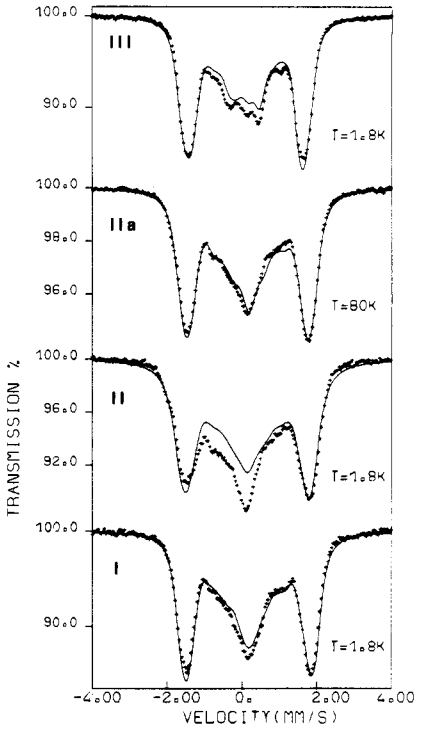

Figure 4. Mössbauer spectra of I–III at H_0 = 80 kOe.

Table IV. Mössbauer Spectral Data for $Fe_4(\mu_3\text{-}S)_3(\mu_3\text{-}S_2)Cp_4$ (I), $[Fe_4(\mu_3\text{-}S)_3(\mu_3\text{-}S_2)Cp_4][PF_6]$ (II), and $[Fe_4(\mu_3\text{-}S)_3(\mu_3\text{-}S_2)Cp_4][PF_6]_2$ (III) at 1.8 K

compd	iron site	%	δ,[a] mm/s	ΔE, mm/S	Γ, mm/s	η[c]
III	Fe(1), Fe(4)	50	0.37 ± 0.02	+1.00	0.28	0.75
	Fe(2)	25	0.43	+0.60	0.32	0.00
	Fe(3)	25	0.24	−0.97	0.28	0.50
II	Fe(1), Fe(4)	50	0.42	−1.09	0.30[b]	0.75
	Fe(2)	25	0.44	+1.21	0.30[b]	0.75
	Fe(3)	25	0.28	+1.25	0.30[b]	0.50
I	Fe(1), Fe(4)	50	0.47	−1.30	0.34	0.70
	Fe(2)	25	0.47	+0.98	0.32	0.50
	Fe(3)	25	0.25	+1.17	0.32	0.75

[a] Relative to natural iron metal at 300 K. [b] Without external field. [c] ±0.1.

(3)–Fe(2)–S(5); 75.07 and 75.43° for Fe(2)–S(5)–Fe(4) and Fe(2)–S(5)–Fe(1).

Mössbauer Properties. Mössbauer spectra of compounds I–III at 1.8 K consist of quadrupole doublets with a varying degree of asymmetry. Representative zero-field spectra are given in Figure 2. Because there was no unambiguous way of assigning the spectral transitions to the different iron sites, Mössbauer experiments in applied longitudinal magnetic fields $H_0 \leq 100$ kOe were carried on. The field dependence of the spectra of I–III at 40 and 80 kOe is shown in Figures 3 and 4, respectively.

Fitting these spectra gives the hyperfine parameters summarized in Table IV, and this was done by assuming three quadrupole doublets for each cluster. A least-squares fit was initially made with two quadrupole doublets with relative intensity ratio 3:1 (three tetracoordinated and one pentacoordinated iron sites) in order to obtain the average values for the hyperfine parameters and to detect any unresolved structure from the line widths.

The spectra of compounds I and III were then fitted with three quadrupole doublets by using Γ line widths close to the instrumental line width and with intensity ratios 2:1:1.

Solid lines in Figures 3 and 4 are computer-generated[20] spectra, with correction for absorber thickness when useful, for fields applied to the randomly oriented powdered samples and with the same quadrupole splittings and isomer shifts as in the zero-field experiments at 1.8 K (see Figure 2). The calculated spectra with total applied field at the nucleus H_n = 40 kOe and H_n = 80 kOe are in good agreement with the experimental spectra. The small difference observed at the central part between experimental and calculated data could be interpreted as a saturation effect due to absorber thickness. Estimating the η values is difficult, and only approximate values are given. The zero-field spectrum of paramagnetic compound II was fitted by analogy with the spectra of compounds I and III (see Table IV). The so-determined hyperfine parameters were used to simulate the experiments with external applied fields. In order to observe this paramagnetic species in both the slow and fast relaxation rate limits and to determine the hyperfine magnetic field H_{hf}, we carried out experiments at different temperatures (1.8–200 K) and with external magnetic fields H_0 up to 100 kOe.

At H_0 = 80 kOe, no changes are observed when the temperature is increased from 80 to 200 K. The theoretical curve is in good agreement with the experimental data (Figure 4), assuming $H_n = H_0$ for all applied fields and with the same line width value (0.30 mm/s) as in the zero-field experiments. Thus, in this range of temperature, the paramagnetic relaxation rate is supposed to be fast and the magnetic splitting has therefore collapsed.

At lower temperatures (1.8–10 K), the introduction of large magnetic fields was expected to induce large hyperfine fields at the iron nuclei of the cluster. Mössbauer experiments at these low temperatures are indeed different from the spectra observed at higher temperatures, but measurement of the separation of the outermost lines by computer simulations gives $H_n = H_0 \pm 5$ kOe over the entire range of applied fields.

Other Physical Properties. The temperature dependence of the reciprocal molar magnetic susceptibility of the monocation II was investigated at 5 kG over the range 6–300 K, and magnetic moment data are reported in Table V (see supplementary material). A diamagnetic correction was applied, calculated to be $\chi_{dia} = -2.5 \times 10^{-4}$ cm^3 mol^{-1}.[12] The μ_{eff} values ranging from 1.67 at 6 K to 1.75 at 300 K, indicate one unpaired electron per monocation tetrametal cluster, assuming spin-only behavior and $S = {}^1/_2$.

^{1}H NMR spectra were run on both the diamagnetic compounds I and III[10] and on the paramagnetic monoxidized species in order to see whether any proton isotropic shifts occur.[21] Indeed, the

(20) Ballet, O. *Hyperfine Interact.* **1985**, *23*, 133.

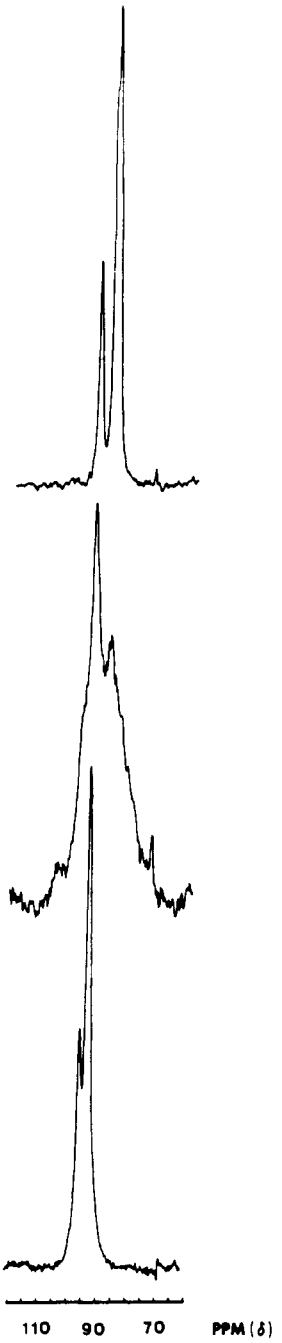

Figure 5. Solid-state ^{13}C NMR spectra of $Fe_4(\mu_3\text{-}S)_3(\mu_3\text{-}S_2)Cp_4$ (I), $[Fe_4(\mu_3\text{-}S)_3(\mu_3\text{-}S_2)Cp_4][PF_6]$ (II), and $[Fe_4(\mu_3\text{-}S)_3(\mu_3\text{-}S_2)Cp_4][PF_6]_2$ (III) at ambient temperature.

cyclopentadienyl protons give one broadened signal, but no isotropic shift is observed. The same occurs in the solid-state ^{13}C NMR spectra (see Figure 5) where only a broadening effect, but no shift, is visible.

Discussion

Our first interest resided in assessing the extent of the electronic influence on the Fe_4S_5 core geometry, by structural comparison of the dication with its less oxidized homologues.[9,11] A slight shortening of the Fe–S bonds is observed when going from the mono- to the dioxidized species: the "short" Fe–S average bond decreases from 2.203 to 2.195 Å; the "long" Fe–S average bond decreases from 2.277 to 2.265 Å. The same occurs with the S(2)–S(4) distance, which moves from 2.067 to 2.056 Å. These are small, but statistically significant changes, which imply that a contraction of the Fe–S core occurs when removing an electron, as already reported by Dahl et al.[18b] and Holm et al.[22] for the $[Fe_4(\mu_3\text{-}S)_4Cp_4]^{0,1+,2+}$ and $[Fe_4(\mu_3\text{-}S)_4(SR)_4]^{2-,3-}$ series.

More substantial are the variations observed in the bonding Fe–Fe interactions: the Fe(1)–Fe(2) and Fe(2)–Fe(4) distances are respectively shortened by 0.06 and 0.21 Å when going from the mono- to the dication. Also, both distances become more equivalent in the dioxidized species. The longer Fe–Fe interactions are also modified, but in a more subtle way (0.01–0.08-Å variation).

These structural variations can be qualitatively related to the cluster orbital occupancy. One can assume that when the dioxidized species is reduced by one electron (compound III → compound II), the extra electron is added to a nonbonding or antibonding tetrametal orbital, which is more centered on Fe(2) and Fe(4) rather than on Fe(1) and Fe(2). This accounts for the lengthening, albeit inequivalent, of the two "short" Fe–Fe distances. The same trend is possibly followed when a second electron is added and to give the neutral homologue. In effect, in the Fe-EXAFS experiments,[11] the Fourier transforms of the experimental and theoretical scattering curves show that the Fe–Fe peak, due to the averaged "short" Fe–Fe distance, moves out from 2.63 Å in the dication (III) to 2.78 Å in the monocation (II) and to 2.95 Å in the neutral homologue (I).

Thus, the successive reduction (or oxidation) steps produce significant structural changes at the Fe(1), Fe(2), and Fe(4) sites but not at the five-coordinated Fe(3) site. It can therefore be assumed that these three Fe centers are more involved in the reduction process than the five-coordinated Fe center.

This assumption is supported by the analysis of the Mössbauer spectral parameters (see Table IV). The average isomer shift value (0.41 mm/s for III, 0.39 mm/s for II, and 0.35 mm/s for I) decreases upon oxidation, which is consistent with a change of iron 3d and 4s electron population, following a removal of electrons from the metal-based molecular orbitals. Such an oxidation level/isomer shift correlation has already been established for analogous complexes[23] and protein clusters. Moreover, at all oxidation states of the system, one doublet has a lower isomer shift value and is nearly invariant upon reduction. This doublet is assigned to the five-coordinated Fe(3) site, which seems not to be affected by the reduction process. Its parameter values (δ and ΔE) are lower than the values reported for other five-coordinated Fe,[6b,7,8,24] but then these parameters can vary substantially with the local geometry, the oxidation state, and the spin state. On the other hand, the three other conventional tetrahedral Fe sites have parameter values that vary jointly upon addition of electrons. This implies that the reduction process is localized predominantly on Fe(1), Fe(2), and Fe(4), as already suggested by the structural results analysis, with a high degree of electron delocalization over these three iron sites.

The large values of η observed in the applied magnetic field spectra are consistent with the nonaxial symmetry of the iron sites. The only exception is Fe(2) in compound III ($\eta = 0$), which is accounted for by the mirror pseudosymmetry put into evidence during the structural analysis of the dicationic cluster.

The detailed experiments performed on the paramagnetic ($S = {}^1/_2$) monocation were designed to study the unpaired spin interaction with the iron centers.

In zero-field experiments, the 1.8 K spectrum consists of three pairs of quadrupole-split lines with the same line width as for the diamagnetic neutral and dicationic parent compounds. The fact

(21) ^1H NMR data for acetonitrile solutions are as follows (in ppm from Me_4Si): −4.86, −4.40 (1:3 intensity ratio) for neutral compound I; −4.56 (broadened signal) for monocationic compound II; −5.83, −5.79, −5.12 (2:1:1 intensity ratio) for dicationic compound III. Solid state ^{13}C NMR data give the following shifts (in ppm from Me_4Si): −92, −86 (1:3; I); −93, −87.5 (broad multiplet; II); −96.5, −93.5 (1:3; III).

(22) Hagen, K. S.; Watson, A. D.; Holm, R. H. *Inorg. Chem.* **1984**, *23*, 2984.
(23) (a) Cammack, R.; Dickson, D. P. E.; Johnson, C. E. In *Iron-Sulfur Proteins*; Lovenberg, W., Ed.; Academic: New York, 1977; Vol. 3, pp 283–330. (b) Christou, G.; Mascharak, P. K.; Armstrong, W. H.; Papaefthymiou, G. C.; Frankel, R. B.; Holm, R. H. *J. Am. Chem. Soc.* **1982**, *104*, 2820.
(24) De Vries, J. L. K. F.; Keijzers, C. P.; De Boer, E. *Inorg. Chem.* **1972**, *11*, 1343.

that neither magnetic hyperfine splitting nor broadening effects are observed at this temperature suggests either a fast paramagnetic relaxation or little spin density at the iron centers.

These alternative explanations can also be used to interpret our experimental results at $T \geq 80$ K and $H_0 \neq 0$ kOe (see Figures 3 and 4). The spectra at 1.8 K with applied field have not yet been interpreted to full satisfaction. The outermost line separation provides evidence for $H_n = H_0 + 5$ kOe. A closer resemblance of the calculated curves with the experimental data was then achieved, assuming a small anisotropic H_{hf} (less than 10 kOe). However, even with this new parameter, we were not able to fully describe the details of the central part of the spectra.

When large magnetic fields are applied to paramagnetic compounds at low temperature, they generally induce a hyperfine magnetic field H_{hf}, by polarization of the unpaired spin, at the iron nuclei, and a long paramagnetic relaxation time ($\geq$100 ns) is expected. Indeed, hyperfine fields of about 100 kOe have been reported for $[Fe_4S_4]$ type clusters.[25,26] When one goes from the fast to the intermediate relaxation rate, a change of the line shape and line width should be observed.

Our experimental data at 1.8 K and $H_0 = 40$ kOe were simulated assuming a higher value ($\Gamma = 0.40$ mm/s) for the outer absorption line width than those used to fit the 80 K spectrum ($\Gamma = 0.30$ mm/s) (see Figures 3 and 4). Always at 1.8 K, the line width remains unchanged when the external field is increased from 60 to 100 kOe. We concluded therefore that $T = 1.8$ K and $H_0 \geq 60$ kOe are good conditions for the system to be at the slow relaxation time limit and that H_{hf} must be quite small. A similar situation has been reported for $[Fe_4S_4Cp_4]^+$[27] and $[Fe_4(CO)_4Cp_4]^+$.[28] These conditions being achieved, we can now suggest that either the unpaired spin does not interact strongly with the iron sites and/or that the three components of H_{hf} average to zero.

The magnetic hyperfine field H_{hf} is comprised of contributions from three sources: The first is the Fermi contact term $\vec{H}_c$—this isotropic contribution of the spin density at the nucleus is usually the most important component ($\sim$−120 kOe per unpaired d electron). The second is the spin dipolar term $\vec{H}_{SD}$, corresponding to the dipolar contribution of the unpaired electronic spins surrounding the nucleus. This anisotropic term reflects the symmetry around the iron nucleus; it has a magnitude of zero for a diamagnetic compound or when the unpaired electron is in an S state, and it is generally small ($\sim$10 kOe) but may in some cases be of the order of 100 kOe.[29] The third source is the orbital term $\vec{H}_L$, due to the orbital motion of the valence electrons.

In our case, since the **g** tensor seems to be almost isotropic ($g = 2.118$, 1.999, and 1.968),[9] the orbital contribution can be neglected. On the other hand, it is not possible at the present time to give a quantitative estimate of $\vec{H}_{SD}$, since it would require a quantitative MO model. As the experimental data involve a very small anisotropic or even zero hyperfine field, one might have assumed that the anisotropic $\vec{H}_{SD}$ nearly cancels the isotropic $\vec{H}_c$. We consider however this hypothesis to be quite unlikely and suggest rather that the unpaired spin does not interact strongly with the iron centers ($\vec{H}_c = -\vec{H}_{SD} \sim 10$ kOe). Such a small interaction could explain the small perturbation of the Mössbauer spectra when the system's conditions change from the fast relaxation limit ($T \geq 80$ K) to the slow relaxation limit ($T = 1.8$ K).

The absence of a large hyperfine interaction may rather indicate a spin delocalization over the cyclopentadienyls or the sulfur atoms. This led us to perform additional ^1H and ^{13}C NMR (solution and solid state) experiments (see Figure 5).[21] The cyclopentadienyl ring protons and carbons show downfield shifts when one goes from the neutral to the dioxidized species. These shifts are suggestive of an overall decrease of the electronic density and further confirm our conclusions from the X-ray distances and Mössbauer data analysis.

Furthermore, looking into the pattern of the resonances, they appear to indicate for the dication (2:1:1 intensity ratio) the presence of two equivalent Fe sites and a third Fe similar to those, while the fourth Fe is clearly different, since the corresponding Cp is upfield-shifted. This last Fe site could correspond to the five-coordinated iron and possibly have a higher electron density. In the case of the neutral compound, this individual Fe site is still present, while the three other Fe sites have become equivalent. Again, these observations are in support of the Mössbauer data analysis.

With the monocation, a broadened resonance is observed, which is due to the proximity of the cyclopentadienyls to the paramagnetic core. No isotropic shifts are observed, however, and one can presume therefore that the unpaired electron spin is not delocalized over the Cp ligands. In support of this, the EPR signal shows no hyperfine structure due to the interactions of the unpaired electron with the cyclopentadienyl H nuclei, and it has a slightly different temperature dependence from those of conventional Fe_4S_4 entities. These exhibit signals that become unobservable above 55 K, owing to rapid electron spin relaxation,[30] whereas $[Fe_4(\mu_3\text{-}S)_3(\mu_3\text{-}S_2)Cp_4]^+$ gives a signal still visible at 120 K.

In conclusion, both the Mössbauer and the NMR studies provide evidence, albeit indirect, for the unpaired electron spin density to be mostly localized on the sulfur centers. This is not inconsistent with the conclusion, drawn from the structural analysis, that the electrons added upon reduction occupy iron centered orbitals. In effect, recent results of an Xα valence bond scattered wave approach, used by Noodleman and co-workers[31] to compute the charge and spin distributions within $[Fe_4S_4(SR)_4]^{2-,3-}$ clusters, show that, upon reduction, most of the added charge (60–70%) migrates to the sulfur atoms. This is a result of changes in orbitals other than those that formally accept the extra electron and that indeed have about 90% iron character.

Acknowledgment. We thank Dr. J. Gaillard, Département de Physique, Centre d'Etudes Nucléaires de Grenoble, for fruitful discussions and suggestions during the course of this study.

Registry No. I, 77589-78-7; II, 77902-72-8; III, 100993-97-3.

Supplementary Material Available: Listings of magnetic moment data for compound II (Table V) and anisotropic thermal parameters, additional interatomic distances and interbond angles, and observed and calculated structure factors for compound III (30 pages). Ordering information is given on any current masthead page.

(25) Evans, M. C. W.; Hall, D. O.; Johnson, C. E. *Biochem. J.* **1970**, *119*, 289.
(26) Moulis, J. M.; Auric, P.; Gaillard, J.; Meyer, J. *J. Biol. Chem.* **1984**, *259*, 11396.
(27) Wong, H.; Sidney, D.; Reiff, W. M.; Frankel, R. B.; Meyer, T. J.; Salmon, D. *Inorg. Chem.* **1978**, *17*, 194.
(28) Frankel, R. B.; Reiff, W. M.; Meyer, T. J.; Cramer, J. L. *Inorg. Chem.* **1974**, *13*, 2515.
(29) Vertes, A.; Korecz, L.; Burger, K. In *Mössbauer Spectroscopy*; Elsevier: Amsterdam, 1979; p 89.
(30) Holm, R. H. In "Iron-Sulfur Proteins; Academic: New York, 1977; p 249.
(31) Noodleman, L.; Norman, J. G.; Osborne, J. H.; Aizman, A.; Case, D. A. *J. Am. Chem. Soc.* **1985**, *107*, 3418.